AGU ADVANCING EARTH AND SPACE SCIENCES

Geophysical Research Letters

RESEARCH LETTER
10.1029/2026GL126477

Aseismic Slip Along the Evaporite-Rich Strike-Slip Katouna-Stamna Fault in Greece

Joel Szrek[1,2], Silvia Crosetto[2], Sabrina Metzger[2], Giorgio Gomba[3], Claudio Faccenna[2,4], and Romain Jolivet[1,5]

[1]Laboratoire de Géologie, Département de Géosciences, École Normale Supérieure, PSL Université, UMR CNRS 8538, Paris, France, [2]GFZ Helmholtz Centre for Geosciences, Potsdam, Germany, [3]German Aerospace Center, Weßling, Germany, [4]Dipartimento di Scienze, Università Roma Tre, Rome, Italy, [5]Institut Universitaire de France, Paris, France

Key Points:

- Aseismic slip along the Katouna-Stamna Fault is confirmed by satellite geodesy, in agreement with field evidence and structural analysis
- The predominant slip direction transitions from pure left-lateral in the south-central part to oblique normal motion in the northern part
- Velocity-weakening material is described along the creeping section suggesting that fluids and pressure-solution creep play a key role

Supporting Information:

Supporting Information may be found in the online version of this article.

Correspondence to:

J. Szrek,
joel.szrek@ens.psl.eu

Citation:

Szrek, J., Crosetto, S., Metzger, S., Gomba, G., Faccenna, C., & Jolivet, R. (2026). Aseismic slip along the evaporite-rich strike-slip Katouna-Stamna Fault in Greece. *Geophysical Research Letters*, *53*, e2026GL126477. https://doi.org/10.1029/2026GL126477

Received 21 AUG 2026
Accepted 1 SEP 2026

Author Contributions:

Conceptualization: Joel Szrek, Silvia Crosetto, Sabrina Metzger, Claudio Faccenna, Romain Jolivet
Data curation: Joel Szrek, Silvia Crosetto, Sabrina Metzger, Giorgio Gomba, Claudio Faccenna
Formal analysis: Joel Szrek, Silvia Crosetto, Sabrina Metzger, Giorgio Gomba, Romain Jolivet
Funding acquisition: Romain Jolivet
Investigation: Joel Szrek, Silvia Crosetto, Sabrina Metzger, Giorgio Gomba, Claudio Faccenna, Romain Jolivet

Abstract Aseismic slip has been observed on many active faults globally, but its controlling mechanisms remain unclear. This study focuses on the NW-striking, left-lateral Katouna-Stamna Fault in Western Greece. We use InSAR surface deformation measurements to confirm the presence of aseismic slip and compare this behavior with structural evidence from field observations. We measure sharp velocity changes across the fault, up to 2 mm/yr in the satellite's ascending and 4 mm/yr in the descending Line-Of-Sight. Kinematic modeling indicates strike-slip rates of up to 19 ± 1 mm/yr, with pure left-lateral slip in the south-central part of the fault transitioning to oblique slip with a normal component in the north. Field data indicate a switch from WNW- to NNW-directed transtension over time. Ductile gypsum deformation suggests that fluids and pressure-solution creep could play a key role in the aseismic fault behavior.

Plain Language Summary The reason why some crustal faults creep slowly without causing earthquakes is not fully understood. We use time-series of radar satellite imagery that monitor crustal motion with millimeter-precision and show that the Katouna-Stamna Fault in Western Greece creeps with up to 19 mm/yr. Numerical simulations confirm that the south-central part of the fault moves sideways, while the northern part shows downward motion, leading to crustal extension. Signs of past movement (called striae) indicate that, over time, the direction of movement has changed. One side of the fault consists of certain soft rocks (such as gypsum) that deform in a slow and flowing way. We suggest that creep could be facilitated here by fluids in the crust.

1. Introduction

Recent advances in satellite-geodetic observation techniques have shown that faults can slip (or creep) slowly and aseismically (Bürgmann, 2018), as well as rapidly, radiating seismic waves during earthquakes. Aseismic slip occurs after large earthquakes (afterslip, e.g., Çakir et al., 2003; Perfettini et al., 2010), during slow-slip events (e.g., Rousset et al., 2016) or precursory phase of large earthquakes (e.g., Socquet et al., 2017; Twardzik et al., 2022), but may also persist over decades (Titus et al., 2006). In addition, aseismic slip modulates elastic strain budget and acts as a barrier to propagation of large ruptures (e.g., Kaneko et al., 2010).

Aseismic slip has been described along continental faults (Jolivet & Frank, 2020), including the San Andreas Fault, California (Steinbrugge et al., 1960), the North Anatolian Fault, Türkiye (Ambraseys, 1970), the Longitudinal Valley Fault, Taiwan (Thomas, Avouac, Champenois, et al., 2014), and the Ilyak Fault in the Tajik Basin (Metzger et al., 2021; Wilkinson et al., 2025). Physical mechanisms underlying occurrence of aseismic slip are debated (Bürgmann, 2018). The frictional resistance of a fault gouge depends on slip velocity, and fault gouge material can induce weakening or strengthening when slip velocity increases (Marone, 1998). Typically, earthquakes are explained by velocity-weakening and aseismic slip by velocity-strengthening friction (Marone, 1998), the latter potentially involving weak minerals (Moore & Rymer, 2007). Other mechanisms invoked to explain slow, aseismic slip are pressure-solution creep, resulting in dissolution of minerals under stress and viscous deformation of rocks (Gratier et al., 2011); large rupture nucleation size, preventing slip rates from reaching dynamic speed (Ampuero & Rubin, 2008); fault geometry complexity (Cattania & Segall, 2021; Romanet et al., 2018); and combination of friction and pressure-solution creep (Bos & Spiers, 2002). These mechanisms are influenced by pressure, temperature, rock type and pore-fluid pressure (Bürgmann, 2018).

Observations of aseismic slip have increased since the launch of the Sentinel-1 mission, which allowed Interferometric Synthetic-Aperture Radar (InSAR) monitoring of tectonically active regions with high spatio-temporal

Methodology: Joel Szrek, Giorgio Gomba, Romain Jolivet
Project administration: Silvia Crosetto, Claudio Faccenna
Resources: Silvia Crosetto, Sabrina Metzger, Claudio Faccenna, Romain Jolivet
Software: Romain Jolivet
Supervision: Silvia Crosetto, Sabrina Metzger, Claudio Faccenna, Romain Jolivet
Validation: Joel Szrek
Visualization: Joel Szrek, Silvia Crosetto, Sabrina Metzger
Writing – original draft: Joel Szrek
Writing – review & editing: Joel Szrek, Silvia Crosetto, Sabrina Metzger, Giorgio Gomba, Claudio Faccenna, Romain Jolivet

resolution and millimeter-precision (e.g., Weiss et al., 2020). In combination with field mapping and structural analysis, geodetic observations of aseismic slip allow identification of mechanisms responsible for such slow fault slip (Thomas, Avouac, Gratier, & Lee, 2014). However, there is little direct evidence that a given rock type controls slip behavior, aside from its mere presence along a creeping section. Along the San Andreas Fault, for example, aseismic slip has been associated with the presence of ophiolites (Irwin & Barnes, 1975), but the creeping section is not fully coated with such rocks, and slip rates strongly depend on friction and gouge structure (Cox et al., 2021), calling for more scrutiny. By showcasing the Katouna-Stamna Fault (KSF) in Greece, we provide evidence that evaporites could directly control nature of slip along this active structure.

Although located in western Greece (Figure 1), one of the most seismically active regions in Europe (Lammers et al., 2023), the KSF is characterized by low seismicity, hence believed to slip aseismically (Pérouse et al., 2017). The fault is embedded in an evaporite-rich environment, characterized mainly by gypsum and salt diapirs (Soto et al., 2024). Experiments suggest that evaporites, particularly gypsum, are velocity-weakening and therefore prone to generating earthquakes (Buijze et al., 2021; Ren, 2024). Contrary to these experiments, geodetic studies find aseismic deformation of large evaporite bodies acting as décollement layers along thrust faults, for example, on the Strophades islets in the Ionian Sea (Stiros, 2005) or in southern Zagros (Palano et al., 2018). These studies emphasize importance of evaporites for aseismic slip on thrust faults, while the KSF and the Tajik Ilyak Fault might be the first examples of similar relationships for strike-slip faulting.

We provide field-based structural observations and a fault slip model from interseismic InSAR rates to constrain long- and short-term kinematics of the KSF. We reconstruct the tectonic evolution of the fault in its geodynamic setting and discuss potential implications and mechanisms explaining aseismic slip on a potentially weakening fault gouge.

2. The Katouna-Stamna Fault and the Ionian-Acarnania Block

The KSF is a 60-km-long, left-lateral transtensional fault system that runs from the Ambracian Gulf to the Patras Gulf in Acarnania region, Western Greece (Figure 1; Basili et al., 2013; Caputo et al., 2012; Ganas et al., 2013; Galanakis et al., 2025; Pérouse et al., 2017; Sboras et al., 2011).

The region has hosted intense seismic activity in the last 20 years (Lammers et al., 2023; Makropoulos et al., 2012), including the 2008 M_w6.4 Movri earthquake (e.g., Papadopoulos et al., 2010; Serpetsidaki et al., 2014), the 2014 M_w6.1/6.0 Cephalonia earthquakes (e.g., Karastathis et al., 2015; Sakkas et al., 2022), the 2015 M_w6.5 Lefkada earthquake (e.g., Melgar et al., 2017; Papadimitriou et al., 2017; Sakkas et al., 2022), and the 2018 M_w6.8 Zakynthos earthquake (e.g., Chousianitis & Konca, 2019; Karakostas et al., 2021; Papadopoulos et al., 2020; Sakkas et al., 2022; Sokos et al., 2020). The KSF, however, shows a remarkable absence of instrumental or historical earthquakes, with the only exception being a M_w5.3 event in 2014 along the northern part of the KSF, whose focal mechanism is consistent with an ENE-dipping left-lateral fault (Figure 1; Dziewonski et al., 1981; Godey et al., 2006; Lammers et al., 2023).

The geodynamic setting of the central-eastern Mediterranean (Figure 1a) is governed by anti-clockwise rotation of Anatolia and consequent southwestward motion of the Aegean (relative to Europe), while subduction of the oceanic-to-continental Adriatic lithosphere along the eastern Adriatic margin (e.g., Chiarabba et al., 2023; Faccenna et al., 2014; Wortel & Spakman, 1992) results in fast oceanic subduction and Hellenic trench retreat to the south (e.g., Catalano et al., 2001; Olive et al., 2014; Pearce et al., 2012) and slow subduction of continental Apulia beneath Albanides-Hellenides to the north of our study region (e.g., D'Agostino et al., 2008; Argnani, 2018; Louvari et al., 1999; Menichelli et al., 2025). The Cephalonia-Lefkada Transform Fault (CLTF), west of Acarnania, roughly marks transition between these two subduction regimes (e.g., Haddad et al., 2020; Louvari et al., 1999; Pérouse et al., 2017).

The KSF, the CLTF, the Movri-Amaliada Fault (MAF), and the subduction backstop front (Pérouse et al., 2017) or other major tectonic structures (Haddad et al., 2020; Vassilakis et al., 2011) delimit an area of low strain and low seismicity often referred to as the 'Ionian-Acarnania Block' (IAB in Figure 1; e.g., Haddad et al., 2020; Pérouse et al., 2017; Vassilakis et al., 2011). The region experienced compression due to the advancing Alpine fold-and-thrust belt and ongoing subduction, followed by extension along the Ambracian Gulf, Lake Trichonida, Patras Gulf and Corinth Rift (Figure 1; Brooks et al., 1988; Underhill, 1989). The KSF connects the Trichonida

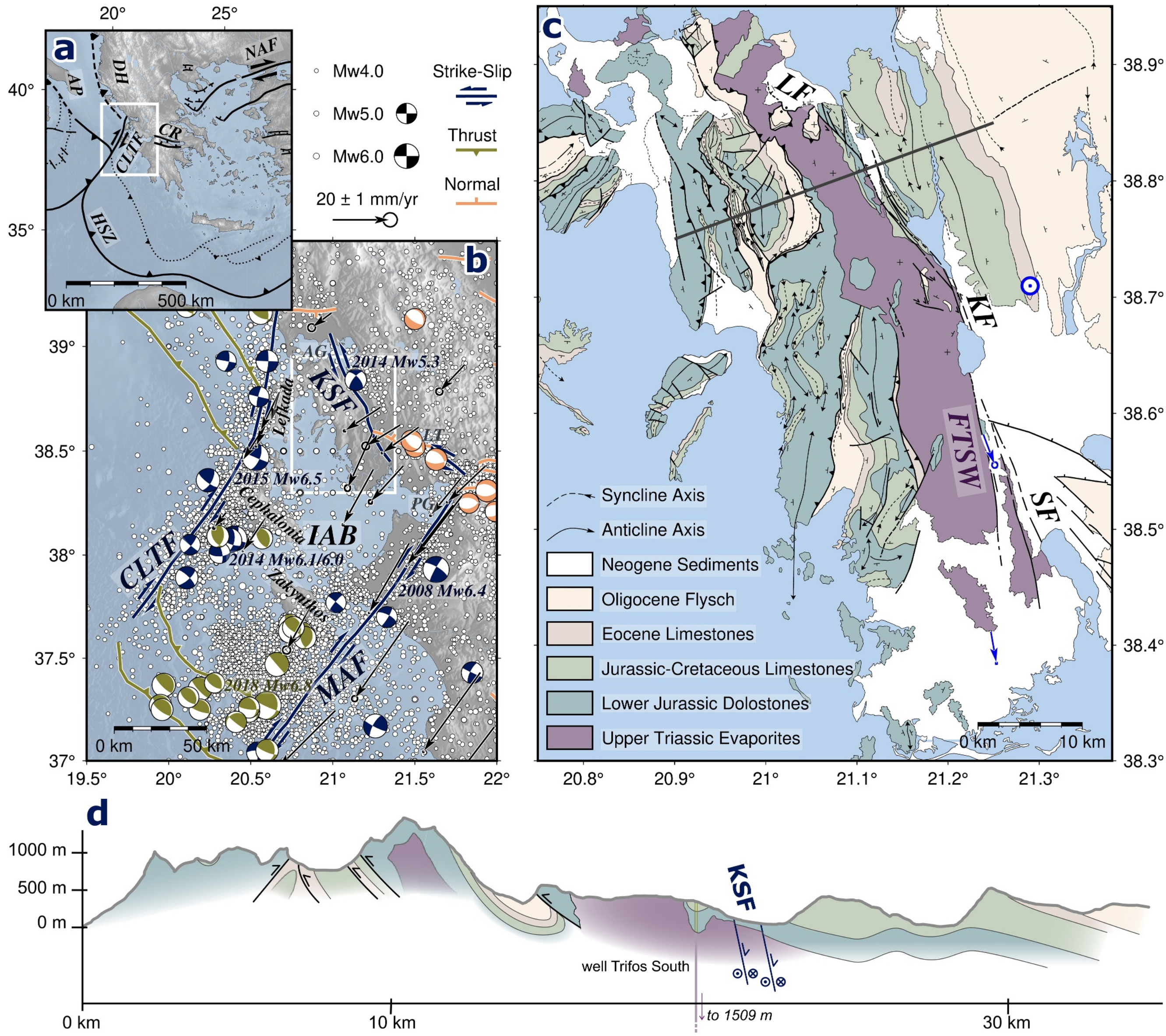

Figure 1. (a) Tectonic map of the Aegean region, after Pérouse et al. (2017), with solid, dashed and dotted lines representing oceanic subduction, continental subduction, and backstop front, respectively. (b) Seismotectonic map of the Ionian-Acarnania region. Continuous lines are fault traces, modified after Sboras et al. (2011); Caputo et al. (2012); Basili et al. (2013). Black arrows are Eurasian-stable GNSS velocities with 2σ confidence intervals (Kenyeres et al., 2019). Focal mechanisms of $M_w > 5$ earthquakes 2005–2025 are from Dziewonski et al. (1981), white dots represent moderate seismicity over the same period (Lammers et al., 2023). Blue, orange and green colors represent strike-slip, normal and thrust tectonics, respectively. White rectangles on panels (a, b) indicate extent of panels (b, c), respectively. (c) Geological map of Acarnania, after Soto et al. (2024). Blue arrows are GNSS velocities relative to the GNSS site shown with blue circle. (d) Structural cross-section across the Katouna-Stamna Fault (KSF) along the profile marked with the gray line on panel (c). Key features include Cephalonia-Lefkada Transform Fault (CLTF), Movri-Amaliada Fault (MAF), Ambracian Gulf (AG), Patras Gulf (PG), Lake Trichonida (LT), North Anatolian Fault (NAF), Corinth Rift (CR), Hellenic Subduction Zone (HSZ), Dinarides-Hellenides (DH), Apulia Platform (AP), Katouna Fault (KF), Stamna Fault (SF), Loutraki Fault (LF) and Fyteies-Trífos Salt Wall (FTSW).

basin to the Ambracian Gulf and the Patras Gulf, with much of its eastern boundary lying within the hanging wall of the north-dipping fault that bounds the Trichonida basin to the south (Figure 1).

The KSF is located in the external part of the Hellenides fold-and-thrust belt, in the Ionian Zone (Figure 1). The Ionian Zone is composed of an Upper Triassic-to-Eocene carbonate sequence organized into three large WSW-vergent thrust sheets, which are detached along underlying Triassic evaporites (Karakitsios & Rigakis, 2007; Soto et al., 2024). Structural cross-sections indicate that evaporites reach depths of up to 10–15 km (Haslinger et al., 1999; Soto et al., 2024; Tselentis et al., 2006). In the Ionian Zone, peculiar salt diapiric structures called 'salt walls' are elongated sub-perpendicularly to the NE-SW-trending shortening direction (Soto et al., 2024). An example is the Fyteies-Trífos Salt Wall (Figure 1), a thick NNW-trending salt wall that separates the Ambracian Gulf from the Patras Gulf and is bound to the east by the KSF for most of its length (Soto et al., 2024). Nearby wells show evaporites up to at least 4,500 m depth (Soto et al., 2024).

The KSF is separated into two main segments (Figure 1): the Katouna Fault (KF) in the north, continuing to the northwest along the strain-releasing Loutraki Fault (LF), and the Stamna Fault (SF) in the south (Pérouse et al., 2017). The KSF exhibits geological slip-rates exceeding 4 mm/yr, based on a Quaternary alluvial fan offset dated through cosmic ray-exposure, while geodetic slip-rates of 10–13 mm/yr were inferred from Global Navigation Satellite System (GNSS) time-series (Bufféral et al., 2026; Pérouse et al., 2017). Based on a distinct rate change across the fault observed in the GNSS velocity field (Figure 1), Pérouse et al. (2017) proposed that the KSF releases strain aseismically.

3. Geologic and Geodetic Evidence for Aseismic Slip

We examine geological motion across the KSF using field evidence and structural analysis. We then constrain short-term geodetic motion by combining published GNSS velocity fields with InSAR velocity maps acquired in two different viewing geometries. We infer a distributed slip model and compare short-term slip-rates with geological observations.

3.1. Field Data Collection and Processing

3.1.1. Methods

We performed structural mapping along the KSF to define the geometry of the fault and its kinematics (Figure S1 and Tables S1–S13 in Supporting Information S1). We systematically measured fault strike and dip; when striae were present, we measured their pitch (rake), and, in case of multiple generations of striae, we determined relative timing of formation through cross-cutting relationships. In addition, we mapped morphotectonic evidence of active tectonics, and lithological observations allowed for interpretation of deformation processes related to aseismic slip.

3.1.2. Results

The KSF trace is highly segmented (Figure 2). The northernmost part of the fault, the LF, is characterized by a clear E-W-striking strain-releasing bend. Between Loutraki and Katouna, the northern KF (nKF) displays a series of left-stepping NW-SE-striking strands. Between Katouna and Fyteies, the central KF (cKF) forms a local transtensional domain marked by the presence of Lake Amvrakia. In its southern section, between Fyteies and Stamna, the southern KF (sKF) branches into several strands linked to Lake Ozeros. To the south, the Stamna Fault (SF) shows even more branching and a less-prominent topographic expression.

Throughout its length, the KSF cuts through carbonates, mainly limestone, in the north, and evaporites, mainly gypsum, in the south (Figures 1, 2c, and 2d). In numerous evaporite outcrops, evidence of ductile deformation includes rocks with shear-related foliation and sheath folds. The abundance of veins, with some cm-size euhedral calcite crystals, indicates significant fluid circulation and overpressure (Chen et al., 2025; Hadizadeh et al., 2024).

On exposed limestone slickensides, up to two generations of striae can be clearly distinguished (Figure 2). On the LF, sub-vertical striae are cross-cut by sub-horizontal ones (Figure 2; stereonet 1), implying a switch from NNW-directed extension to E-W conjugate movement with respect to the main KSF. The nKF displays sub-horizontal striae cross-cut by more oblique ones (Figure 2; stereonet 2), indicating a switch from pure strike-slip to oblique-slip motion. Along the cKF, a NNW-striking slickenside shows large sub-horizontal grooves with dm-wavelength overprinted by more oblique cm-size striations with ∼345° azimuth (Figures 2a and 2b; stereonet 3), consistent with a change from pure strike-slip motion to oblique-slip motion. To the south, a smaller WNW-striking splay shows WNW-ESE sub-horizontal striae cross-cut by SW-trending ones (Figure 2; stereonet 4), possibly implying that the plane formed as a conjugate Riedel plane switching from strike-slip to dip-slip motion in a releasing bend. Striations on other step-overs show oblique-slip motion along fault planes, with ∼330° azimuth (Figure 2; stereonets 5–6). Fault planes along the sKF become less clear, and their striations do not show cross-cutting relationships (Figure 2; stereonets 7–11). In this part of the fault, striae with inconsistent kinematics can be observed within short distance. Low-quality outcrops characterize the SF, which lacks clear kinematic indicators (Figure 2; stereonets 12–13).

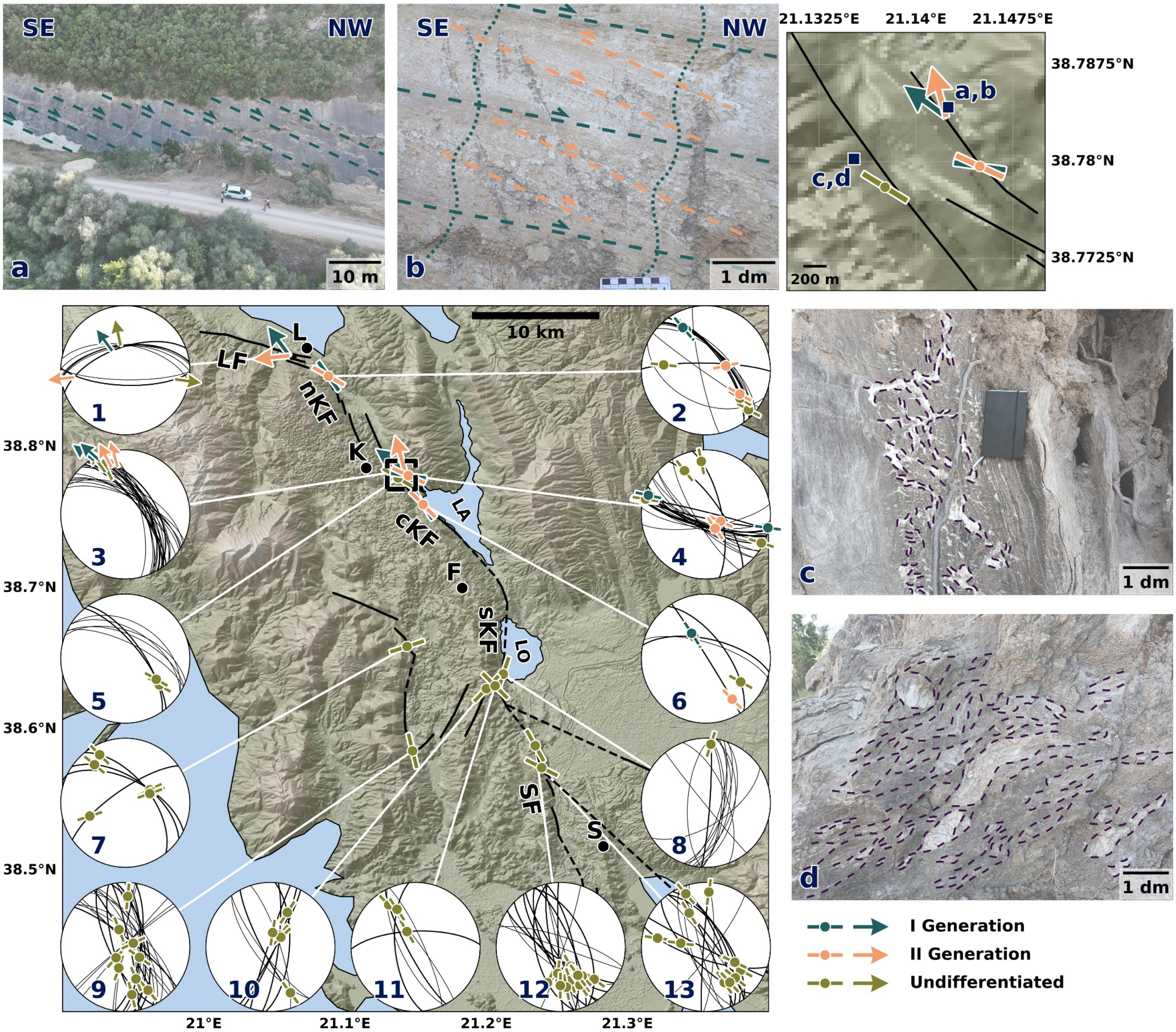

Figure 2. Map with stereonets and trend of striations. Arrows represent striae color-coded by relative age (I generation if older, II generation if younger). Undifferentiated striations represent an unresolved population. Solid and dashed lines represent confirmed and inferred fault traces, respectively. Towns/villages are Loutraki (L), Katouna (K), Fyteies (F) and Stamna (S). The black dashed rectangle east of Katouna indicates extent of zoomed-in panel in upper right corner. Key features include Loutraki Fault (LF), northern Katouna Fault (nKF), central Katouna Fault (cKF), southern Katouna Fault (sKF), Stamna Fault (SF), Lake Amvrakia (LA) and Lake Ozeros (LO). Blue squares in zoomed-in panel represent locations of field photos, showing (a) drone image of fault plane with (b) cross-cutting striae indicating transition from nearly pure left-lateral (in blue) to oblique normal left-lateral slip (in orange), (c) ductile flow of gypsum around dolostone layers and (d) gypsum-rich ductile deformation with shear-related foliation.

Overall, structural observations indicate a first kinematic regime dominated by strike-slip motion along the KSF overprinted by transtensional kinematics, favoring oblique slip within a roughly N-S-oriented extensional stress field.

3.2. Surface Motion From Satellite Geodesy

3.2.1. Methods

To constrain the deformation rates across the KSF in detail, we combine several published GNSS velocity fields of the region with full-coverage InSAR rate maps acquired in two view directions.

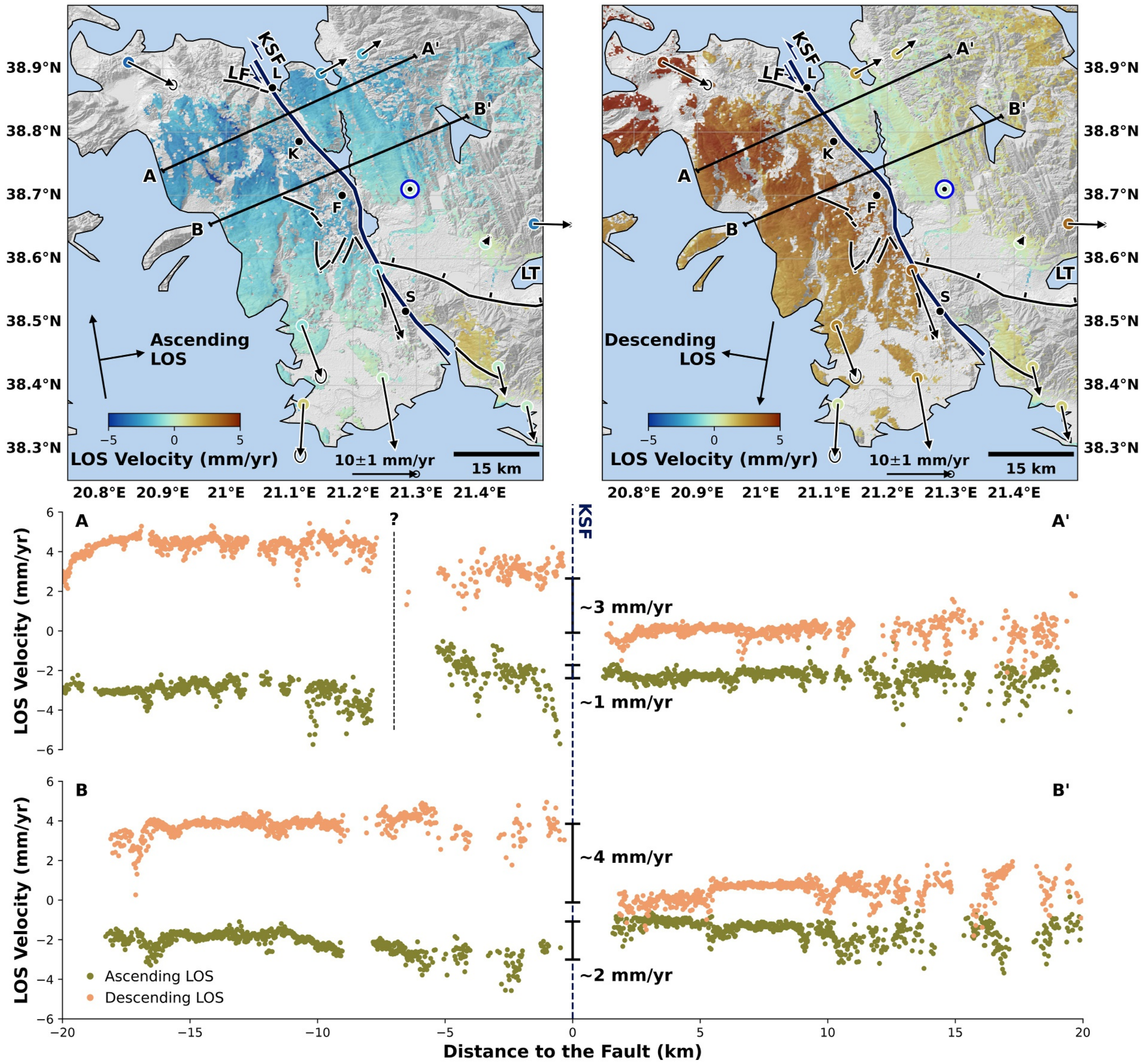

Figure 3. Top Panels: Ascending and descending InSAR LOS velocity maps of Sentinel-1 radar imagery 2016–2022. Higher values indicate motion toward the satellite. Black arrows mark horizontal GNSS velocities relative to the GNSS site shown with a blue circle (Floyd et al., 2010; Kenyeres et al., 2019; Serpelloni et al., 2022), colored dots represent GNSS LOS velocities. Solid lines mark the Katouna-Stamna Fault (KSF) and secondary faults after Sboras et al. (2011); Caputo et al. (2012); Basili et al. (2013) and our mapping. Key features include Loutraki Fault (LF) and Lake Trichonida (LT). Towns/villages abbreviated as in Figure 2. Bottom panels: Ascending (green) and descending (orange) fault-perpendicular LOS rates on profiles AA′ and BB′ as marked in top panels. Dashed lines mark the KSF and a potential secondary fault (?).

We combine the horizontal GNSS velocity fields of Kenyeres et al. (2019), Serpelloni et al. (2022), and Floyd et al. (2010), using a Helmert transformation in the European Terrestrial Reference System 2000 (Boucher et al., 2004; Helmert, 1876). This solution alignment is based on 50 common sites in Greece with a resulting adjustment of solutions precise down to 1 mm/yr.

InSAR time-series were built from Sentinel-1 radar imagery acquired from 2016 to 2022 on ascending track 80 and descending track 175 (Gomba et al., 2024). We use a persistent and distributed scatterer approach with inversion of full-covariance matrices to avoid potential biases due to misclosure in vegetated areas (Ansari et al., 2017; Gonzalez et al., 2013; Plattner et al., 2022). Processing includes corrections for ionospheric effects, solid-earth tides, and tropospheric delays (Cong, 2014; Cong et al., 2018; Gonzalez et al., 2018), and unwrapping of interferometric phase in time and space. Line-Of-Sight (LOS) velocities are inferred from ascending and descending displacement time-series (Figures S2–S4 in Supporting Information S1 and Supporting Informations

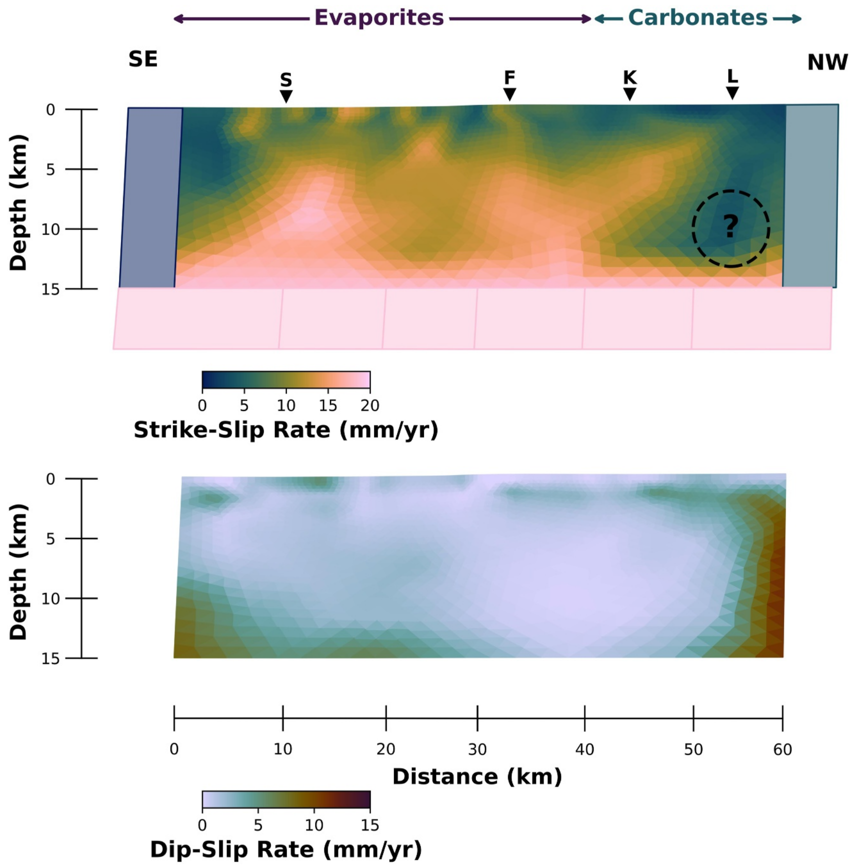

Figure 4. Distributed slip model for strike-slip (top) and dip-slip (bottom) components. Rectangles extending the fault laterally and toward depth account for boundary effects. Dashed circle with '?' marks a potentially locked patch. The predominant lithologies along the KSF trace reported above the top plot are after Soto et al. (2024). Towns/villages abbreviated as in Figure 2.

S2 and S3) accounting for seasonal signals. Finally, we reference the LOS velocity maps to the GNSS reference frame by removing an offset between the GNSS velocities projected in LOS and the InSAR LOS velocities averaged within 1-km-radius of each GNSS site (Metzger et al., 2021). The final accuracy of this adjustment is 1 mm/yr.

From the LOS velocity maps we extract cross-fault profiles every 250 m (e.g., Figure 3) and, where possible, calculate the velocity difference across the fault to estimate surface slip-rates and uncertainties (Figure S5 in Supporting Information S1). Standard deviations in inferred LOS velocities are below 1 mm/yr. Since the fault strike is almost parallel to the satellite's ascending flight direction, ascending track data are less sensitive to fault-parallel motion than descending ones.

3.2.2. Results

The deformation signal is clearly visible in the InSAR data across the KSF and to a lesser extent across Lake Trichonida; however, no deformation differences are observable across the LF due to its proximity to coastline (Figure 3). Across the KSF, descending LOS velocities show a sharp decay of up to 4 mm/yr over a distance of <1 km, while ascending LOS rates increase by up to 2 mm/yr over the same distance, indicative of shallow locking or aseismic slip at the surface (e.g., Jolivet et al., 2012; Jolivet et al., 2023). The offset sign change between the two LOS velocity fields indicates primarily horizontal motion, except for the northernmost section (Figure S5 in Supporting Information S1).

A second rate change of ~2 mm/yr in both LOS highlights a secondary active fault branch ~7 km west of the nKF (Figure 3). To the southeast, velocity difference could not be directly calculated from profiles as resolvable velocity gradients are sparse and InSAR-derived deformation patterns may be influenced by ∼N-S-extension across Lake Trichonida.

3.3. Distributed Slip-Rate Modeling

3.3.1. Methods

We use the Classic Slip Inversion (CSI) library (Jolivet et al., 2015) to infer slip-rates at depth. To reduce computational costs and avoid data redundancy, we downsample ascending and descending LOS InSAR velocity maps using a quadtree-based approach, masking out pixels closer than 1 km from the fault trace to avoid averaging motion across the fault (Lohman & Simons, 2005). We evaluate covariance of each data set by estimating exponential covariance functions (Figure S6 in Supporting Information S1) in an area far from the fault (Sudhaus & Jónsson, 2009). We restrict our data set to 12 GNSS sites near the KSF (Figure S1 and Table S14 in Supporting Information S1).

We project the fault at depth assuming a 75° dip toward the ENE, in agreement with field measurements, and use a slightly updated fault trace from Sboras et al. (2011); Caputo et al. (2012); Basili et al. (2013). We discretize the fault plane into triangles with depth-dependent size from <1 km^2 to >17 km^2 (Figure S7 in Supporting Information S1) using DistMesh (Persson & Strang, 2004). Below 15 km (brittle–ductile transition) we apply uniform motion on an infinitely deep dislocation (Savage & Burford, 1973) on a 65° ENE-dipping plane in agreement with the moment tensor solution of the M_w5.3 event in 2014. We expand our fault segment along-strike with auxiliary rectangular patches to account for edge effects. Slip at the bottom of our fault are equal to those of the infinite auxiliary segment at depth. The Green's functions relate unit slip on the segments to surface displacement assuming a stratified elastic half-space (Zhu & Rivera, 2002). For the shallow section of the KSF we use linear interpolating Green's functions tied to nodes of the triangular fault mesh and a piecewise constant slip distribution on each rectangular element of the model (Jolivet et al., 2023). Additional parameters minimize the offsets between InSAR and GNSS observations.

We use a Bayesian approach (Bayes, 1958) and chose uninformative uniform priors (e.g., 0–25 mm/yr for slip-rate). A Gaussian likelihood function accounts for data and epistemic uncertainties (Jolivet et al., 2023). The AlTar sampler draws 60,000 posterior samples and explores the model parameter space without explicit smoothing.

3.3.2. Results

The posterior probability density function resembles a normal distribution (Figure S8 in Supporting Information S1) with mean slip varying along strike and dip (Figure 4). Uncertainties are roughly constant, around 7 mm/yr (Figure S9 in Supporting Information S1). Aseismic slip extends to the surface and increases toward depth (Figure S10 in Supporting Information S1). Our preferred model exhibits strike-slip rates of 19 ± 1 mm/yr on the deep part of the fault (15 km depth). At 10 km depth, the fault slips at 13 ± 7 mm/yr in its southern and 15 ± 7 mm/yr in its central part, while in the northern part the KSF appears locked with uncertainties larger than slip values. At 5 km depth, strike-slip rates reach 11 ± 7 mm/yr in the southern part, 12 ± 7 mm/yr in the central part and 7 ± 6 mm/yr in the northern part. Significant dip-slip is only visible in the northern part, reaching 5 ± 4 mm/yr at intermediate depth and 10 ± 7 mm/yr at deeper depths. At the surface, strike-slip rate reaches up to 13 ± 5 mm/yr in the southern part, 10 ± 2 mm/yr in the central part, and 2 ± 1 mm/yr in the northern part, with 3 ± 1 mm/yr of dip-slip in the northern part. Thus, pure sinistral shear in the south-central part transitions to oblique normal motion in the northern part. The only potentially locked patch at depth is located in the northern part of the KSF, corresponding to the area where the fault mainly crosses carbonates instead of evaporites (Soto et al., 2024).

4. Discussion

4.1. Fault Model Uncertainty

Our model shows a good data fit, with Root-Mean-Square misfit between observations and predictions of 4 mm/yr. GNSS residuals are highest at the northern end of the fault (Figure S11 and Table S15 in Supporting Information S1), where InSAR residuals are rather small (Figures S12 and S13 in Supporting Information S1). This discrepancy may arise from variable data coverage. In the south, the GNSS network is denser than in the north, whereas InSAR data are more sparse. Note that only horizontal GNSS rates have been included in the model, which are almost insensitive to the dip-slip component in the north.

The change from evaporites to carbonates across and along the fault implies a variation of elastic properties, possibly including ductile deformation, which our model does not account for. Poor fit in the northwest and southeast of the InSAR rate maps could result from unmodeled deformation of the CLTF and extension across Lake Trichonida (Figure 3), respectively.

Previous studies suggest a uniform strike-slip rate of 10–13 mm/yr (Bufféral et al., 2026; Pérouse et al., 2017). Our model exhibits variable slip-rates, with rapid strike-slip motion of up to 13 ± 5 mm/yr near the surface in the south-central part and more oblique-slip motion in the northern part, as expected from our observations (Figures S5 and S12 in Supporting Information S1). At intermediate depths, our model suggests strike-slip rates of up to 15 ± 7 mm/yr in the south-central part, and a locked patch to the north (Figure 4), which corresponds to location of the 2014 M_w5.3 earthquake (Godey et al., 2006). The significant difference from previously published rates most likely arises from data coverage, as our data provide dense coverage of the whole area, whereas previous studies were limited only to a GNSS network (Bufféral et al., 2026; Pérouse et al., 2017).

4.2. Geological Versus Satellite-Geodetic Observations

The KSF surface trace is more localized and prominent in the north than in the south. This could result from: lithological contrast, as carbonates in the north build more pronounced geomorphic expression than evaporites and loose sediments in the south; oblique slip in the north favoring larger fault scarps than lateral slip to the south, in agreement with the increased normal component to the north in our kinematic model; lower fault maturity in the south, supported by inconsistent kinematic indicators and higher segmentation; or a combined effect of lithological contrast, fault kinematics, and maturity.

The KSF trace segmentation observed in the field is not entirely reflected in the InSAR rates. This may be related to observational data gaps, such as cultivated areas, as well as to spatial resolution of InSAR rates.

Geological observations provide information on fault kinematic evolution over time. The younger generation of NNW-trending striae shows mostly oblique-slip motion with dominant strike-slip component, in agreement with geodetic observations. This indicates that geological kinematic regime under which they formed may be recent and possibly still in place. However, WNW-trending striae of unknown age disagree with geodetic observations and might be related to older fault activity.

The KSF could provide information on the regional kinematic evolution. The CLTF probably formed at 8–6 (Royden & Papanikolaou, 2011) to 5–3 (Crosetto et al., 2025) Ma, either through differential slab rollback driven by along-strike variations in slab buoyancy (Royden & Papanikolaou, 2011), or by westward propagation of the North Anatolian Fault into the Aegean region (Papanikolaou & Royden, 2007). The second scenario would involve a progressive onset of deformation from the North Anatolian Fault to the CLTF through active rifts and the KSF (Vassilakis et al., 2011). However, the Late Pliocene age of the oldest sediments underlying the Ambracian and Trichonida grabens (Vassilakis et al., 2011) suggests that the KSF transtensional system formed after the CLTF, which challenges the North Anatolian Fault westward propagation theory.

The switch from WNW- to NNW-motion along the KSF, indicated by our structural data, could be related to the KSF initial role as strike-slip link between grabens, driven by extension along the Corinth Rift at 3–4 Ma (L. Jolivet et al., 2013) and later transferred to the Patras Gulf, Lake Trichonida and Ambracian Gulf (Brooks et al., 1988; Tranos et al., 2020; Underhill, 1989). Progressive segmentation in this area, facilitated by the presence of evaporites, could then lead to slip partitioning from the KSF toward the basins, favoring a more transtensional regime and culminating in present-day kinematics depicted by our InSAR data.

4.3. Drivers of Aseismic Slip

Currently, there are few reported cases of aseismic slip along strike-slip faults hosted in evaporite-rich sequences, another example being the Ilyak Fault in the Tajik Basin (Metzger et al., 2021; Wilkinson et al., 2025). Similarly to Western Greece, the Tajik Basin has been affected by compression and salt tectonics, resulting in active salt structures (Metzger et al., 2021) with evaporite-rich layers favoring aseismic slip on the Ilyak Fault (Wilkinson et al., 2025). This consistency would support a more general interpretation that evaporite-rich shear zones may systematically promote aseismic slip, but additional factors, such as fluids or stress regime, might also play a role. From our observations, limited to the surface, the presence of evaporites appears crucial. Although structural cross-sections suggest that evaporites can reach depths of up to 15 km, available nearby wells are not deep enough to provide direct evidence for evaporites below 5 km depth (Soto et al., 2024). Haslinger et al. (1999) find high seismic velocities at seismogenic depths in the northern part of the KSF and low velocities in its south-central part, velocity anomalies that correlate with our aseismic slip distribution and could be interpreted as either the presence of evaporites or fluids.

Aseismic slip is commonly associated with the presence of velocity-strengthening materials (Moore & Rymer, 2007). However, dominant lithology along the KSF is gypsum, characterized by velocity-weakening properties (Buijze et al., 2021; Ren, 2024), suggesting that not all creeping faults are necessarily made of velocity-strengthening materials.

Another explanation for aseismic slip along the KSF could be widespread fluid circulation, as indicated by abundant veins we observed along the fault. Elevated pore-fluid pressure is known to stabilize slip either by reducing effective normal stress and, consequently, increasing nucleation size, preventing slip from reaching seismic velocities (Ampuero & Rubin, 2008), or by dilatant strengthening (Segall et al., 2010). Furthermore, while frictional behavior of anhydrite-dolomite fault gouges is velocity-weakening in dry samples, its behavior becomes velocity-strengthening in wet samples (Pluymakers et al., 2016). The hypothesis of large fluid circulation seems plausible given the location of the KSF between rift systems and possibly above a subduction zone (Bocchini et al., 2018). Fluids could also originate from dehydration of gypsum, causing aseismic slip by pore-fluid pressure build-up due to low permeability (Leclère et al., 2016).

Ductile deformation at shallow depth resulting from interactions between evaporites and fluids may also be involved. Although dry gypsum does not display aseismic behavior on its own, pressure-solution creep has been described in wet gypsum (de Meer & Spiers, 1997). While in brittle regime salt shows fast and regular stick-slip motion with velocity-weakening behavior, in semi-brittle regime it shows slower slip and smaller stress drops with velocity-strengthening behavior (Hirauchi et al., 2020). Experiments of ductile shear within evaporite-bearing rocks suggest that slip may reach rates compatible with those observed along active faults (de Meer & Spiers, 1997). Pressure-solution creep is facilitated by high solubility of evaporites and the presence of fluids, and could explain ductile deformation, abundant veining, and correlation between evaporites and aseismic slip (Figures 2 and 4). Pressure solution is slower between identical minerals due to healed boundaries, but faster between different minerals, notably halite and calcite (Zubtsov et al., 2004), which would explain why deformation localizes along the contact between evaporites and carbonates, possibly on both sides of the salt wall. In addition, pressure-solution creep has been reported in the gouge of other creeping faults, that is, the San Andreas Fault (Gratier et al., 2011), the North Anatolian Fault (Kaduri et al., 2019), and the Longitudinal Valley Fault (Thomas, Avouac, Gratier, & Lee, 2014). Effectively, aseismic slip could result from a combination of frictional sliding and pressure-solution creep (Bos & Spiers, 2002). Regardless of underlying mechanism, fluids seem to play a crucial role in aseismic slip along the KSF.

In conclusion, based on available evidence, both ductile deformation of evaporites and fluid overpressure (or a combination of the two) could explain aseismic slip along the KSF.

5. Conclusions

By combining geological fieldwork with geodetic displacement rates and slip modeling, we find evidence of oblique aseismic slip along the KSF. The kinematic consistency between geological record and modern geodetic observations suggests long-lived aseismic slip along the KSF, likely facilitated by subsurface evaporites.

Aseismic slip of the KSF occurs in velocity-weakening materials and may be driven by fluids interacting with evaporites, as suggested by abundant veins and ductile deformation. Future work will require absolute dating of the KSF activity and further investigation of fluid circulation in this area.

Conflict of Interest

The authors declare no conflicts of interest relevant to this study.

Availability Statement

GNSS velocities are provided by Kenyeres et al. (2019), Serpelloni et al. (2022), and Floyd et al. (2010). InSAR rate maps (Gomba et al., 2024) are provided as Supporting Informations S2 and S3 and have been created from modified Copernicus Sentinel-1 data 2016–2022 (Torres et al., 2012), acquired and distributed by the European Space Agency (ESA), and available for download here: https://dataspace.copernicus.eu/data-collections/copernicus-sentinel-missions/sentinel-1. The CSI kinematic model library and the AlTar sampler (Jolivet et al., 2015) are available on GitHub. We used the Generic Mapping Tools (Wessel et al., 2019), Python and the Scientific Color Maps (Crameri, 2018) for figures.

Acknowledgments

The authors thank Ambrosio Vega Ruiz for his support and advice in the field. Joel Szrek thanks Manon Dalaison for correcting his internship report, which would later turn into this manuscript, as well as her valuable insights and fruitful discussion. The authors also thank the editor Fabio A. Capitanio for handling this manuscript as well as Christoph Grützner and Sotiris Sboras for investing their time and thoughts in improving the quality of this work. Part of this work was supported by the European Research Council (ERC) projects Geo4D (758210) and iQuake (101125232) under the European Union's Horizon 2020 Framework Program for Research and Innovation. Romain Jolivet acknowledges funding from the Alexander von Humboldt Foundation and from the Institut Universitaire de France. Open Access funding enabled and organized by Projekt DEAL.

References

Ambraseys, N. N. (1970). Some characteristic features of the Anatolian fault zone. *Tectonophysics*, *9*(2–3), 143–165. https://doi.org/10.1016/0040-1951(70)90014-4

Ampuero, J.-P., & Rubin, A. M. (2008). Earthquake nucleation on rate and state faults–aging and slip laws. *Journal of Geophysical Research*, *113*(B1). https://doi.org/10.1029/2007JB005082

Ansari, H., De Zan, F., & Bamler, R. (2017). Sequential estimator: Toward efficient InSAR time series analysis. *IEEE Transactions on Geoscience and Remote Sensing*, *55*(10), 5637–5652. https://doi.org/10.1109/TGRS.2017.2711037

Argnani, A. (2018). Subduction evolution of the Dinarides and the Cretaceous orogeny in the Eastern Alps: Hints from a new paleotectonic interpretation. *Tectonics*, *37*(2), 621–635. https://doi.org/10.1002/2017TC004632

Basili, R., Kastelic, V., Demircioglu, M., Garcia Moreno, D., Nemser, E., & Petricca, P. (2013). The european Database of seismogenic faults (EDSF) compiled in the framework of the project SHARE. https://doi.org/10.6092/INGV.IT-SHARE-EDSF

Bayes, T. (1958). An essay towards solving a problem in the doctrine of chances. *Biometrika*, *45*(3–4), 296–315. https://doi.org/10.1093/biomet/45.3-4.296

Bocchini, G., Brüstle, A., Becker, D., Meier, T., Van Keken, P., Ruscic, M., et al. (2018). Tearing, segmentation, and backstepping of subduction in the Aegean: New insights from seismicity. *Tectonophysics*, *734*, 96–118. https://doi.org/10.1016/j.tecto.2018.04.002

Bos, B., & Spiers, C. J. (2002). Frictional-viscous flow of phyllosilicate-bearing fault rock: Microphysical model and implications for crustal strength profiles. *Journal of Geophysical Research*, *107*(B2), ECV–1. https://doi.org/10.1029/2001JB000301

Boucher, C., Altamimi, Z., Sillard, P., & Feissel-Vernier, M. (2004). The ITRF2000 (Vol. *31*).

Brooks, M., Clews, J., Melis, N., & Underhill, J. (1988). Structural development of Neogene basins in western Greece. *Basin Research*, *1*(3), 129–138. https://doi.org/10.1111/j.1365-2117.1988.tb00010.x

Bufféral, S., Briole, P., Chamot-Rooke, N., & Pubellier, M. (2026). Slip rates, diffuse deformation and interseismic loading in central and southwestern Greece, from GNSS velocities. *Geophysical Journal International*, *247*(1), ggag229. https://doi.org/10.1093/gji/ggag229

Buijze, L., Guo, Y., Niemeijer, A., Ma, S., & Spiers, C. (2021). Effects of heterogeneous gouge segments on the slip behavior of experimental faults at dm scale. *Earth and Planetary Science Letters*, *554*, 116652. https://doi.org/10.1016/j.epsl.2020.116652

Bürgmann, R. (2018). The geophysics, geology and mechanics of slow fault slip. *Earth and Planetary Science Letters*, *495*, 112–134. https://doi.org/10.1016/j.epsl.2018.04.062

Çakir, Z., Chabalier, J.-B. d., Armijo, R., Meyer, B., Barka, A., & Peltzer, G. (2003). Coseismic and early post-seismic slip associated with the 1999 Izmit earthquake (Turkey), from SAR interferometry and tectonic field observations. *Geophysical Journal International*, *155*(1), 93–110. https://doi.org/10.1046/j.1365-246X.2003.02001.x

Caputo, R., Chatzipetros, A., Pavlides, S., & Sboras, S. (2012). The Greek database of seismogenic sources (GreDaSS): State-of-the-art for northern Greece. *Annals of Geophysics*, *55*(5), 859–894. https://doi.org/10.4401/ag-5168

Catalano, R., Doglioni, C., & Merlini, S. (2001). On the mesozoic Ionian basin. *Geophysical Journal International*, *144*(1), 49–64. https://doi.org/10.1046/j.0956-540X.2000.01287.x

Cattania, C., & Segall, P. (2021). Precursory slow slip and foreshocks on rough faults. *Journal of Geophysical Research: Solid Earth*, *126*(4), e2020JB020430. https://doi.org/10.1029/2020JB020430

Chen, S., Liu, X., Wang, R., Wei, L., Liu, B., & Bao, H. (2025). An experimental study of dolostone recrystallization under fluid overpressure and its implication for reservoir property improvement. *Minerals*, *15*(3), 230. https://doi.org/10.3390/min15030230

Chiarabba, C., Menichelli, I., Bianchi, I., Giacomuzzi, G., & De Gori, P. (2023). Continental subduction of Adria in the Apennines and relation with seismicity and hazard. *Frontiers in Earth Science*, *11*, 1253443. https://doi.org/10.3389/feart.2023.1253443

Chousianitis, K., & Konca, A. O. (2019). Intraslab deformation and rupture of the entire subducting crust during the 25 October 2018 Mw 6.8 Zakynthos earthquake. *Geophysical Research Letters*, *46*(24), 14358–14367. https://doi.org/10.1029/2019GL085845

Cong, X. (2014). *SAR interferometry for volcano monitoring: 3D-PSI analysis and mitigation of atmospheric refractivity*. (Doctoral dissertation). Technische Universität München. Retrieved from https://mediatum.ub.tum.de/1198042

Cong, X., Balss, U., Rodriguez Gonzalez, F., & Eineder, M. (2018). Mitigation of tropospheric delay in SAR and InSAR using NWP data: Its validation and application examples. *Remote Sensing*, *10*(10), 1515. https://doi.org/10.3390/rs10101515

Cox, S., Ikari, M. J., MacLeod, C. J., & Fagereng, Å. (2021). Frictional characteristics of oceanic transform faults: Progressive deformation and alteration controls seismic style. *Geophysical Research Letters*, *48*(24), e2021GL096292. https://doi.org/10.1029/2021GL096292

Crameri, F. (2018). Scientific colour maps. *Zenodo*, *10*, 5281. https://doi.org/10.5281/zenodo.1243862

Crosetto, S., Faccenna, C., Ballato, P., Mouslopoulou, V., Begg, J., Shen, C.-C., & Hu, H.-M. (2025). Kinematic evolution of the Cephalonia-Lefkada transform fault zone: Strain partitioning in response to subduction margin dynamics. *Tectonics*, *44*(10), e2025TC008862. https://doi.org/10.1029/2025TC008862

D'Agostino, N., Avallone, A., Cheloni, D., D'Anastasio, E., Mantenuto, S., & Selvaggi, G. (2008). Active tectonics of the Adriatic region from GPS and earthquake slip vectors. *Journal of Geophysical Research*, *113*(B12). https://doi.org/10.1029/2008JB005860

de Meer, S., & Spiers, C. J. (1997). Uniaxial compaction creep of wet gypsum aggregates. *Journal of Geophysical Research*, *102*(B1), 875–891. https://doi.org/10.1029/96JB02481

Dziewonski, A. M., Chou, T.-A., & Woodhouse, J. H. (1981). Determination of earthquake source parameters from waveform data for studies of global and regional seismicity. *Journal of Geophysical Research*, *86*(B4), 2825–2852. https://doi.org/10.1029/JB086iB04p02825

Faccenna, C., Becker, T. W., Auer, L., Billi, A., Boschi, L., Brun, J. P., et al. (2014). Mantle dynamics in the Mediterranean. *Reviews of Geophysics*, *52*(3), 283–332. https://doi.org/10.1002/2013RG000444

Floyd, M., Billiris, H., Paradissis, D., Veis, G., Avallone, A., Briole, P., et al. (2010). A new velocity field for Greece: Implications for the kinematics and dynamics of the Aegean. *Journal of Geophysical Research*, *115*(B10). https://doi.org/10.1029/2009JB007040

Galanakis, D., Sboras, S., Sakellariou, D., Pavlides, S., Iordanidou, K., & Georgiou, C. (2025). The Hellenic DataBase of active faults (HeDBAF): A new, national geodatabase of active faults for the broader Greek territory. In *EGU General Assembly Conference abstracts* (pp. EGU25–9230). https://doi.org/10.5194/egusphere-egu25-9230

Ganas, A., Oikonomou, I., & Tsimi, C. (2013). NOAfaults: A digital database for active faults in Greece. *Bulletin of the Geological Society of Greece*, *47*(2), 518–530. https://doi.org/10.12681/bgsg.11079

Godey, S., Bossu, R., Guilbert, J., & Mazet-Roux, G. (2006). The Euro-Mediterranean Bulletin: A comprehensive seismological Bulletin at regional scale. *Seismological Research Letters*, *77*(4), 460–474. https://doi.org/10.1785/gssrl.77.4.460

Gomba, G., De Zan, F., Brcic, R., & Eineder, M. (2024). Mapping worldwide ground deformation in high-strain areas with SAR PS/DS interferometry and Sentinel-1 imagery. *European Geosciences Union General Assembly*, *2024*(EGU24), 8645. https://doi.org/10.5194/egusphere-egu24-8645

Gonzalez, F. R., Adam, N., Parizzi, A., & Brcic, R. (2013). The integrated wide area processor (IWAP): A processor for wide area persistent scatterer interferometry. In *ESA living planet symposium* (Vol. 722).353

Gonzalez, F. R., Parizzi, A., & Brcic, R. (2018). Evaluating the impact of geodetic corrections on interferometric deformation measurements. In *EUSAR 2018; 12th European conference on synthetic aperture radar* (pp. 1–5).

Gratier, J.-P., Richard, J., Renard, F., Mittempergher, S., Doan, M.-L., Di Toro, G., et al. (2011). Aseismic sliding of active faults by pressure solution creep: Evidence from the San Andreas Fault observatory at depth. *Geology*, *39*(12), 1131–1134. https://doi.org/10.1130/G32073.1

Haddad, A., Ganas, A., Kassaras, I., & Lupi, M. (2020). Seismicity and geodynamics of western Peloponnese and central Ionian Islands: Insights from a local seismic deployment. *Tectonophysics*, *778*, 228353. https://doi.org/10.1016/j.tecto.2020.228353

Hadizadeh, J., Boyle, A. P., & Gaughan, A. E. (2024). A study of fluid overpressure microstructures from the creeping segment of the San Andreas fault. *Journal of Structural Geology*, *180*, 105065. https://doi.org/10.1016/j.jsg.2024.105065

Haslinger, F., Kissling, E., Ansorge, J., Hatzfeld, D., Papadimitriou, E., Karakostas, V., et al. (1999). 3D crustal structure from local earthquake tomography around the Gulf of Arta (Ionian region, NW Greece). *Tectonophysics*, *304*(3), 201–218. https://doi.org/10.1016/S0040-1951(98)00298-4

Helmert, F. (1876). Die Genauigkeit der Formel von Peters zur Berechnung des wahrscheinlichen Beobachtungsfehlers directer Beobachtungen gleicher Genauigkeit. *Astronomische Nachrichten*, *88*(8), 113–131. https://doi.org/10.1002/asna.18760880802

Hirauchi, K.-i., Yoshida, Y., Yabe, Y., & Muto, J. (2020). Slow stick-slip failure in halite gouge caused by brittle-plastic fault heterogeneity. *Geochemistry, Geophysics, Geosystems*, *21*(9), e2020GC009165. https://doi.org/10.1029/2020GC009165

Irwin, W. P., & Barnes, I. (1975). Effect of geologic structure and metamorphic fluids on seismic behavior of the San Andreas fault system in central and northern California. *Geology*, *3*(12), 713–716. https://doi.org/10.1130/0091-7613(1975)3<713:eogsam>2.0.co;2

Jolivet, L., Faccenna, C., Huet, B., Labrousse, L., Le Pourhiet, L., Lacombe, O., et al. (2013). Aegean tectonics: Strain localisation, slab tearing and trench retreat. *Tectonophysics*, *597*, 1–33. https://doi.org/10.1016/j.tecto.2012.06.011

Jolivet, R., & Frank, W. (2020). The transient and intermittent nature of slow slip. *AGU Advances*, *1*(1), e2019AV000126. https://doi.org/10.1029/2019AV000126

Jolivet, R., Jara, J., Dalaison, M., Rouet-Leduc, B., Özdemir, A., Dogan, U., et al. (2023). Daily to centennial behavior of aseismic slip along the central section of the North Anatolian Fault. *Journal of Geophysical Research: Solid Earth*, *128*(7), e2022JB026018. https://doi.org/10.1029/2022JB026018

Jolivet, R., Lasserre, C., Doin, M.-P., Guillaso, S., Peltzer, G., Dailu, R., et al. (2012). Shallow creep on the Haiyuan fault (Gansu, China) revealed by SAR interferometry. *Journal of Geophysical Research*, *117*(B6). https://doi.org/10.1029/2011JB008732

Jolivet, R., Simons, M., Agram, P., Duputel, Z., & Shen, Z.-K. (2015). Aseismic slip and seismogenic coupling along the central San Andreas Fault. *Geophysical Research Letters*, *42*(2), 297–306. https://doi.org/10.1002/2014GL062222

Kaduri, M., Gratier, J.-P., Lasserre, C., Çakir, Z., & Renard, F. (2019). Quantifying the partition between seismic and aseismic deformation along creeping and locked sections of the North Anatolian Fault, Turkey. *Pure and Applied Geophysics*, *176*(3), 1293–1321. https://doi.org/10.1007/s00024-018-2027-2

Kaneko, Y., Avouac, J.-P., & Lapusta, N. (2010). Towards inferring earthquake patterns from geodetic observations of interseismic coupling. *Nature Geoscience*, *3*(5), 363–369. https://doi.org/10.1038/ngeo843

Karakitsios, V., & Rigakis, N. (2007). Evolution and petroleum potential of Western Greece. *Journal of Petroleum Geology*, *30*(3), 197–218. https://doi.org/10.1111/j.1747-5457.2007.00197.x

Karakostas, V., Tan, O., Kostoglou, A., Papadimitriou, E., & Bonatis, P. (2021). Seismotectonic implications of the 2020 Samos, Greece, M w 7.0 mainshock based on high-resolution aftershock relocation and source slip model. *Acta Geophysica*, *69*(3), 979–996. https://doi.org/10.1007/s11600-021-00580-y

Karastathis, V., Mouzakiotis, E., Ganas, A., & Papadopoulos, G. (2015). High-precision relocation of seismic sequences above a dipping moho: The case of the January–February 2014 seismic sequence on Cephalonia island (Greece). *Solid Earth*, *6*(1), 173–184. https://doi.org/10.5194/se-6-173-2015

Kenyeres, A., Bellet, J., Bruyninx, C., Caporali, A., De Doncker, F., Droscak, B., et al. (2019). Regional integration of long-term national dense GNSS network solutions. *GPS Solutions*, *23*(4), 1–17. https://doi.org/10.1007/s10291-019-0902-7

Lammers, S., Weatherill, G., Grünthal, G., & Cotton, F. (2023). EMEC-2021-The European-Mediterranean Earthquake Catalogue–version 2021. https://doi.org/10.5880/GFZ.EMEC.2021.001

Leclère, H., Faulkner, D., Wheeler, J., & Mariani, E. (2016). Permeability control on transient slip weakening during gypsum dehydration: Implications for earthquakes in subduction zones. *Earth and Planetary Science Letters*, *442*, 1–12. https://doi.org/10.1016/j.epsl.2016.02.015

Lohman, R. B., & Simons, M. (2005). Some thoughts on the use of InSAR data to constrain models of surface deformation: Noise structure and data downsampling. *Geochemistry, Geophysics, Geosystems*, *6*(1). https://doi.org/10.1029/2004GC000841

Louvari, E., Kiratzi, A., & Papazachos, B. (1999). The Cephalonia transform fault and its extension to western Lefkada Island (Greece). *Tectonophysics*, *308*(1–2), 223–236. https://doi.org/10.1016/S0040-1951(99)00078-5

Makropoulos, K., Kaviris, G., & Kouskouna, V. (2012). An updated and extended earthquake catalogue for Greece and adjacent areas since 1900. *Natural Hazards and Earth System Sciences*, *12*(5), 1425–1430. https://doi.org/10.5194/nhess-12-1425-2012

Marone, C. (1998). Laboratory-derived friction laws and their application to seismic faulting. *Annual Review of Earth and Planetary Sciences*, *26*(1), 643–696. https://doi.org/10.1146/annurev.earth.26.1.643

Melgar, D., Ganas, A., Geng, J., Liang, C., Fielding, E. J., & Kassaras, I. (2017). Source characteristics of the 2015 Mw6. 5 Lefkada, Greece, strike-slip earthquake. *Journal of Geophysical Research: Solid Earth*, *122*(3), 2260–2273. https://doi.org/10.1002/2016JB013452

Menichelli, I., De Gori, P., Funiciello, F., & Claudio, C. (2025). The two-sided continental subduction of the Adria microplate (Mediterranean). *Geology*, *53*(4), 296–300. https://doi.org/10.1130/G52556.1

Metzger, S., Gągała, Ł., Ratschbacher, L., Lazeckỳ, M., Maghsoudi, Y., & Schurr, B. (2021). Tajik depression and greater Pamir neotectonics from InSAR rate maps. *Journal of Geophysical Research: Solid Earth*, *126*(12), e2021JB022775. https://doi.org/10.1029/2021JB022775

Moore, D. E., & Rymer, M. J. (2007). Talc-bearing serpentinite and the creeping section of the San Andreas fault. *Nature*, *448*(7155), 795–797. https://doi.org/10.1038/nature06064

Olive, J.-A., Pearce, F., Rondenay, S., & Behn, M. D. (2014). Pronounced zonation of seismic anisotropy in the Western Hellenic subduction zone and its geodynamic significance. *Earth and Planetary Science Letters*, *391*, 100–109. https://doi.org/10.1016/j.epsl.2014.01.029

Palano, M., Imprescia, P., Agnon, A., & Gresta, S. (2018). An improved evaluation of the seismic/geodetic deformation-rate ratio for the Zagros fold-and-thrust collisional belt. *Geophysical Journal International*, *213*(1), 194–209. https://doi.org/10.1093/gji/ggx524

Papadimitriou, E., Karakostas, V., Mesimeri, M., Chouliaras, G., & Kourouklas, C. (2017). The Mw6. 5 17 November 2015 Lefkada (Greece) earthquake: Structural interpretation by means of the aftershock analysis. *Pure and Applied Geophysics*, *174*(10), 3869–3888. https://doi.org/10.1007/s00024-017-1601-3

Papadopoulos, G. A., Agalos, A., Minadakis, G., Triantafyllou, I., & Krassakis, P. (2020). Short-term foreshocks as key information for mainshock timing and rupture: The Mw6. 8 25 October 2018 Zakynthos earthquake, Hellenic subduction zone. *Sensors*, *20*(19), 5681. https://doi.org/10.3390/s20195681

Papadopoulos, G. A., Karastathis, V., Kontoes, C., Charalampakis, M., Fokaefs, A., & Papoutsis, I. (2010). Crustal deformation associated with east Mediterranean strike–slip earthquakes: The 8 June 2008 Movri (NW Peloponnese), Greece, earthquake (Mw6. 4). *Tectonophysics*, *492*(1–4), 201–212. https://doi.org/10.1016/j.tecto.2010.06.012

Papanikolaou, D. J., & Royden, L. H. (2007). Disruption of the Hellenic arc: Late Miocene extensional detachment faults and steep Pliocene-Quaternary normal faults—Or what happened at Corinth? *Tectonics*, *26*(5). https://doi.org/10.1029/2006TC002007

Pearce, F. D., Rondenay, S., Sachpazi, M., Charalampakis, M., & Royden, L. H. (2012). Seismic investigation of the transition from continental to oceanic subduction along the western Hellenic Subduction zone. *Journal of Geophysical Research*, *117*(B7). https://doi.org/10.1029/2011JB009023

Perfettini, H., Avouac, J.-P., Tavera, H., Kositsky, A., Nocquet, J.-M., Bondoux, F., et al. (2010). Seismic and aseismic slip on the Central Peru megathrust. *Nature*, *465*(7294), 78–81. https://doi.org/10.1038/nature09062

Pérouse, E., Sébrier, M., Braucher, R., Chamot-Rooke, N., Bourlès, D., Briole, P., et al. (2017). Transition from collision to subduction in Western Greece: The Katouna–Stamna active fault system and regional kinematics. *International Journal of Earth Sciences*, *106*(3), 967–989. https://doi.org/10.1007/s00531-016-1345-9

Persson, P.-O., & Strang, G. (2004). A simple mesh generator in MATLAB. *SIAM Review*, *46*(2), 329–345. https://doi.org/10.1137/S0036144503429121

Plattner, C., Parizzi, A., Carena, S., Rieger, S. M., Friedrich, A. M., Abolghasem, A. M., & DeZan, F. (2022). Long-lived afterslip of the 2013 M w 6.1 Minab earthquake detected by Persistent scatterer interferometry along the Irer fault (western Makran-Zagros transition zone, Iran). *Geophysical Journal International*, *229*(1), 171–185. https://doi.org/10.1093/gji/ggab456

Pluymakers, A., Niemeijer, A., & Spiers, C. (2016). Frictional properties of simulated anhydrite-dolomite fault gouge and implications for seismogenic potential. *Journal of Structural Geology*, *84*, 31–46. https://doi.org/10.1016/j.jsg.2015.11.008

Ren, D. (2024). Friction stabilities of gypsum and kaolinite/calcite mixture fault gauges under high pressure. *Frontiers in Earth Science*, *11*, 1346880. https://doi.org/10.3389/feart.2023.1346880

Romanet, P., Bhat, H. S., Jolivet, R., & Madariaga, R. (2018). Fast and slow slip events emerge due to fault geometrical complexity. *Geophysical Research Letters*, *45*(10), 4809–4819. https://doi.org/10.1029/2018GL077579

Rousset, B., Jolivet, R., Simons, M., Lasserre, C., Riel, B., Milillo, P., et al. (2016). An aseismic slip transient on the North Anatolian Fault. *Geophysical Research Letters*, *43*(7), 3254–3262. https://doi.org/10.1002/2016GL068250

Royden, L. H., & Papanikolaou, D. J. (2011). Slab segmentation and late Cenozoic disruption of the Hellenic arc. *Geochemistry, Geophysics, Geosystems*, *12*(3). https://doi.org/10.1029/2010GC003280

Sakkas, V., Kapetanidis, V., Kaviris, G., Spingos, I., Mavroulis, S., Diakakis, M., et al. (2022). Seismological and ground deformation study of the Ionian Islands (W. Greece) during 2014–2018, a period of intense seismic activity. *Applied Sciences*, *12*(5), 2331. https://doi.org/10.3390/app12052331

Savage, J., & Burford, R. (1973). Geodetic determination of relative plate motion in central California. *Journal of Geophysical Research*, *78*(5), 832–845. https://doi.org/10.1029/JB078i005p00832

Sboras, S., Pavlides, S., Caputo, R., Chatzipetros, A., Michailidou, A., Valkaniotis, S., & Papathanasiou, G. (2011). Improving the resolution of seismic hazard estimates for critical facilities: The database of Greek crustal seismogenic sources in the frame of the SHARE project. In *Proceedings of the 30 Convegno Nazionale GNGTS* (Vol. 1417).

Segall, P., Rubin, A. M., Bradley, A. M., & Rice, J. R. (2010). Dilatant strengthening as a mechanism for slow slip events. *Journal of Geophysical Research*, *115*(B12). https://doi.org/10.1029/2010JB007449

Serpelloni, E., Cavaliere, A., Martelli, L., Pintori, F., Anderlini, L., Borghi, A., et al. (2022). Surface velocities and strain-rates in the Euro-Mediterranean region from massive GPS data processing. *Frontiers in Earth Science*, *10*, 907897. https://doi.org/10.3389/feart.2022.907897

Serpetsidaki, A., Elias, P., Ilieva, M., Bernard, P., Briole, P., Deschamps, A., et al. (2014). New constraints from seismology and geodesy on the M w= 6.4 2008 Movri (Greece) earthquake: Evidence for a growing strike-slip fault system. *Geophysical Journal International*, *198*(3), 1373–1386. https://doi.org/10.1093/gji/ggu212

Socquet, A., Valdes, J. P., Jara, J., Cotton, F., Walpersdorf, A., Cotte, N., et al. (2017). An 8 month slow slip event triggers progressive nucleation of the 2014 Chile megathrust. *Geophysical Research Letters*, *44*(9), 4046–4053. https://doi.org/10.1002/2017GL073023

Sokos, E., Gallovič, F., Evangelidis, C. P., Serpetsidaki, A., Plicka, V., Kosteleckỳ, J., & Zahradník, J. (2020). The 2018 M w 6.8 Zakynthos, Greece, earthquake: Dominant strike-slip faulting near subducting slab. *Seismological Research Letters*, *91*(2A), 721–732. https://doi.org/10.1785/0220190169

Soto, J., Tranos, M., Bega, Z., Dooley, T., Hernández, P., Hudec, M., et al. (2024). Contrasting styles of salt-tectonic processes in the Ionian zone (Greece and Albania): Integrating surface geology, subsurface data, and experimental models. *Tectonics*, *43*(1), e2023TC008104. https://doi.org/10.1029/2023TC008104

Steinbrugge, K. V., Zacher, E. G., Tocher, D., Whitten, C., & Claire, C. (1960). Creep on the San Andreas fault. *Bulletin of the Seismological Society of America*, *50*(3), 389–415. https://doi.org/10.1785/BSSA0500030389

Stiros, S. C. (2005). Geodetic evidence for mobilization of evaporites during the 1997 Strophades (W Hellenic Arc) Mw 6.5 earthquake. *Journal of Geophysics and Engineering*, *2*(2), 111–117. https://doi.org/10.1088/1742-2132/2/2/005

Sudhaus, H., & Jónsson, S. (2009). Improved source modelling through combined use of InSAR and GPS under consideration of correlated data errors: Application to the June 2000 Kleifarvatn earthquake, Iceland. *Geophysical Journal International*, *176*(2), 389–404. https://doi.org/10.1111/j.1365-246X.2008.03989.x

Thomas, M. Y., Avouac, J.-P., Champenois, J., Lee, J.-C., & Kuo, L.-C. (2014). Spatiotemporal evolution of seismic and aseismic slip on the Longitudinal Valley Fault, Taiwan. *Journal of Geophysical Research: Solid Earth*, *119*(6), 5114–5139. https://doi.org/10.1002/2013JB010603

Thomas, M. Y., Avouac, J.-P., Gratier, J.-P., & Lee, J.-C. (2014). Lithological control on the deformation mechanism and the mode of fault slip on the Longitudinal Valley Fault, Taiwan. *Tectonophysics*, *632*, 48–63. https://doi.org/10.1016/j.tecto.2014.05.038

Titus, S. J., DeMets, C., & Tikoff, B. (2006). Thirty-five-year creep rates for the creeping segment of the San Andreas fault and the effects of the 2004 Parkfield earthquake: Constraints from alignment arrays, continuous global positioning system, and creepmeters. *Bulletin of the Seismological Society of America*, *96*(4B), S250–S268. https://doi.org/10.1785/0120050811

Torres, R., Snoeij, P., Geudtner, D., Bibby, D., Davidson, M., Attema, E., et al. (2012). GMES Sentinel-1 mission. *Remote Sensing of Environment*, *120*, 9–24. https://doi.org/10.1016/j.rse.2011.05.028

Tranos, M. D., Weber, J. C., Bussey, J., & O'Sullivan, P. (2020). Trichonis basin, western central Greece: Is it an immature basin in the Corinth Rift or a pull-apart in a sinistral rift–trench link? *Journal of the Geological Society*, *177*(1), 120–140. https://doi.org/10.1144/jgs2018-213

Tselentis, G.-A., Sokos, E., Martakis, N., & Serpetsidaki, A. (2006). Seismicity and seismotectonics in Epirus, western Greece: Results from a microearthquake survey. *Bulletin of the Seismological Society of America*, *96*(5), 1706–1717. https://doi.org/10.1785/0120020086

Twardzik, C., Duputel, Z., Jolivet, R., Klein, E., & Rebischung, P. (2022). Bayesian inference on the initiation phase of the 2014 Iquique, Chile, earthquake. *Earth and Planetary Science Letters*, *600*, 117835. https://doi.org/10.1016/j.epsl.2022.117835

Underhill, J. R. (1989). Late Cenozoic deformation of the Hellenide foreland, western Greece. *Geological Society of America Bulletin*, *101*(5), 613–634. https://doi.org/10.1130/0016-7606(1989)101<0613:lcdoth>2.3.co;2

Vassilakis, E., Royden, L., & Papanikolaou, D. (2011). Kinematic links between subduction along the Hellenic trench and extension in the Gulf of Corinth, Greece: A multidisciplinary analysis. *Earth and Planetary Science Letters*, *303*(1–2), 108–120. https://doi.org/10.1016/j.epsl.2010.12.054

Weiss, J. R., Walters, R. J., Morishita, Y., Wright, T. J., Lazecky, M., Wang, H., et al. (2020). High-resolution surface velocities and strain for Anatolia from Sentinel-1 InSAR and GNSS data. *Geophysical Research Letters*, *47*(17), e2020GL087376. https://doi.org/10.1029/2020GL087376

Wessel, P., Luis, J. F., Uieda, L. a., Scharroo, R., Wobbe, F., Smith, W. H., & Tian, D. (2019). The generic mapping tools version 6. *Geochemistry, Geophysics, Geosystems*, *20*(11), 5556–5564. https://doi.org/10.1029/2019GC008515

Wilkinson, R., Daout, S., Walker, R., Dodds, N., & Ischuk, A. (2025). Aseismic slip on the Ilyak Strike-slip fault (Tajikistan) and active fault and landslide hazards in and around the Tajik Basin revealed by InSAR. *Tectonics*, *44*(12), e2025TC008860. https://doi.org/10.1029/2025TC008860

Wortel, M., & Spakman, W. (1992). Structure and dynamics of subducted lithosphere in the Mediterranean region. In *Proceedings of the koninklijke nederlandse akademie van wetenschappen: Biological, chemical, geophysical, physical and medical sciences* (pp. 325–347). KNAW.

Zhu, L., & Rivera, L. A. (2002). A note on the dynamic and static displacements from a point source in multilayered media. *Geophysical Journal International*, *148*(3), 619–627. https://doi.org/10.1046/j.1365-246X.2002.01610.x

Zubtsov, S., Renard, F., Gratier, J.-P., Guiguet, R., Dysthe, D. K., & Traskine, V. (2004). Experimental pressure solution compaction of synthetic halite/calcite aggregates. *Tectonophysics*, *385*(1–4), 45–57. https://doi.org/10.1016/j.tecto.2004.04.016